Autonomous station keeping for LEO missions with a hybrid continuous/impulsive electric propulsion system

IEPC-2011-287

Presented at the 32nd International Electric Propulsion Conference, Wiesbaden, Germany September 11–15, 2011

Andrea Garulli[*] and Antonio Giannitrapani[†]
Università degli Studi di Siena, Siena, 53100, Italy

Mirko Leomanni[‡] Fabrizio Scortecci[§]
Aerospazio Tecnologie s.r.l., Rapolano Terme, Siena, 53040, Italy

In this paper, the problem of autonomous orbit control is addressed, for a spacecraft driven by an electric propulsion system composed of a Hall effect thruster and a resistojet. The considered reference mission is a low Earth orbit typical for observation satellites. An extended Kalman filter processes the measurements coming from GPS, gyro and star-tracker sensors, in order to estimate the spacecraft position and velocity. A hybrid continuous/impulsive control scheme is implemented to track the desired reference signals. The effectiveness of the proposed system is analyzed via numerical simulations.

[*] Professor, Dipartimento di Ingegneria dell'Informazione, garulli@ing.unisi.it.
[†] Assistant Professor, Dipartimento di Ingegneria dell'Informazione, giannitrapani@ing.unisi.it.
[‡] Research Engineer, Aerospazio Tecnologie s.r.l., leomanni@libero.it.
[§] Chairman, Aerospazio Tecnologie s.r.l., fscortecci@aerospazio.com.

Nomenclature

$\mathbf{a}$	=	Spacecraft acceleration, m/s^2
a	=	Semi-major axis, m
e	=	Orbit eccentricity
e_x	=	Eccentricity vector x-component
e_y	=	Eccentricity vector y-component
f	=	Scale factor bias, ppm
g	=	Standard gravity, m/s^2
$\mathbf{I}$	=	Inertia matrix
I	=	Specific impulse, s
i	=	Orbit inclination, rad
M	=	Mean anomaly, rad
m	=	Spacecraft mass, kg
$\mathbf{p}_u$	=	Thrust, N
$\mathbf{q}_{IB}$	=	Quaternion, Inertial $\rightarrow$ Body frame
$\mathbf{R}_{IE}$	=	Rotation matrix, Inertial $\rightarrow$ ECEF frame
$\mathbf{R}(\mathbf{q})$	=	Rotation matrix from a quaternion $\mathbf{q}$
$\mathbf{r}$	=	Spacecraft position, m
u	=	Spacecraft mean argument of latitude, rad
$\mathbf{v}$	=	Spacecraft velocity, m/s
$\Delta\mathbf{v}_u$	=	Impulsive delta-v, m/s
$\delta\mathbf{q}(\,\cdot\,)$	=	Quaternion from a small rotation
$\boldsymbol{\epsilon}$	=	Alignment error, rad
μ	=	Earth gravitational parameter, m^3/s^2
$\boldsymbol{\tau}_u$	=	Spacecraft torque, Nm
ω	=	Argument of perigee, rad
$\boldsymbol{\omega}$	=	Spacecraft angular velocity, rad/s
Ω	=	Right ascension of the ascending node, rad

Superscripts

B	=	Vector expressed in the body frame
E	=	Vector expressed in the ECEF frame
$\downarrow$	=	Time instant before an impulsive burn
$\uparrow$	=	Time instant after an impulsive burn

Accents

$\vee$	=	Measured values
$\wedge$	=	Estimated values

Other symbols

$\mathbf{I}_{j\times k}$	=	Identity matrix with j rows and k columns
$\circ$	=	Quaternion product
$[\boldsymbol{\omega}\times]$	=	Skew-symmetric matrix from vector $\boldsymbol{\omega}$

I. Introduction

Nowadays, electric propulsion (EP) is widely recognized as a successful technology for a large class of missions. Thanks to its high specific impulse, EP is largely adopted in many commercial geostationary satellites and deep space missions.[1–5] On the contrary, only few studies have focused on EP for low Earth orbit (LEO) missions. Nevertheless, besides challenging scientific missions requiring drag free spacecraft operations,[6–9] there are also many LEO missions that have a potential commercial interest, like Earth observation by means of small and cheap satellites.[10]

Maintaining a given low Earth orbit traditionally requires frequent ground-based control actions, in order to compensate for atmospheric drag and other perturbative forces. For small, low cost satellites, ground-in-the-loop control can be a dominant element of both cost and risk.[11] In addition, it is typically based on impulsive control schemes, thus resulting in limited satellite lifetime due to the the large amount of delta-v needed. The combined use of new low power EP technologies and autonomous GNC techniques can provide an effective way to address these issues, thanks to significant savings on the propellant mass and lower spacecraft operation costs.

In this work, we investigate the application of an EP system for autonomous station-keeping of a given low Earth orbit, performed by an observation minisatellite carrying an electro-optical payload. The EP system is based on a single Xenon propellant bus, shared by a low power Hall effect thruster and a resistojet. The former features a high specific impulse and provides continuous low thrust in the tangential direction, while the latter generates a higher thrust level to perform out-of-plane impulsive maneuvers. This results in a hybrid continuous/impulsive control scheme. Attitude stabilization is addressed using three momentum wheels. The navigation solution is based on an extended Kalman filter that estimates position and attitude of the spacecraft from the available gyro, star-tracker and GPS measurements. A control law based on the mean orbital elements is used for orbit control, while a proportional-derivative feedback law is employed for attitude control. The reference mission has been simulated in order to validate the proposed GNC solution and to evaluate the performance of the propulsion system, in terms of achievable accuracy, Hall thruster and resistojet operating regime and propellant mass consumption.

The paper is organized as follows. In Section II, the reference mission considered in the paper is described. Section III introduces the dynamic model adopted for the spacecraft, together with a description of the sensor and actuator characteristics. In Section IV, the guidance, navigation and control system developed for the proposed mission is briefly illustrated. Section V reports results of numerical simulations. In Section VI, some conclusions are drawn and future directions of research are outlined.

II. Reference mission

The objective of the reference mission is to maintain the nominal orbit and attitude of a small remote sensing satellite, with given accuracy and lifetime requirements, through a suitable autonomous GNC technique. In the following, details of the mission, navigation requirements, and spacecraft configuration, are provided.

A. Orbit and attitude

The reference mission orbit is a specialized sun-synchronous, repeat ground-track and frozen orbit, which is a common design for low Earth observation satellites.[12] The orbit is nearly circular, with an altitude of around 233 km, which corresponds to a 11-day ground track repeat period. The initial orbital elements are derived by using a simplified J2 and J3 zonal harmonics analysis and refined through numerical simulations, ignoring all the periodic orbital perturbations.[13] Since the orbit is nearly circular, the eccentricity vector and mean argument of latitude replace the eccentricity, argument of perigee and mean anomaly. Table 1 shows the initial nominal values of the mean orbital elements for the chosen reference mission.

The reference orbit is defined in such a way that gravitational perturbations, which cause the sun synchronous secular motion of $\dot{\Omega} = 360°/\text{year}$, do not need to be counteracted. As a consequence, the propulsion system is activated only to compensate for non gravitational disturbances, by means of orbital elements control.[14] The dominant non gravitational perturbing forces on the reference orbit are due to atmospheric drag and resonance effects induced by the Sun. The most significant effects of these perturbations on the orbital elements are a constant decay in the semi-major axis, in the order of 300 m per revolution, and a minor secular inclination drift.

Table 1. Orbital elements (initial nominal values)

Semi-major axis	a	6596.285 km
Inclination	i	96.403°
Eccentricity vector x-component	$e_x = e\cos\omega$	0
Eccentricity vector y-component	$e_y = e\sin\omega$	0.0011
Right ascension of the ascending node	Ω	10°
Mean argument of latitude	$u = M + \omega$	$270° + 90° = 0°$

The spacecraft is nominally aligned with a Frenet frame along the orbit. This is a rotating frame centered at the satellite center of mass, and therefore it is not inertial. In this work, the X axis is always tangential to the orbit, aligned to the velocity vector of the spacecraft. The Y axis is normal to the orbital plane, being parallel with the angular momentum vector ($\mathbf{h} = \mathbf{r} \times \mathbf{v}$). The Z axis completes the reference frame ($Z = X \times Y$) and it is always aligned with the position vector for circular orbits. The X, Y and Z axes define the in-track, cross-track and normal directions. The in-track and normal directions are approximately aligned to the along-track and radial directions of a local vertical/local horizontal (LVLH) frame for nearly circular orbits.

B. Navigation and control requirements

On-board sensors and actuators are selected in order to meet the navigation and control accuracy requirements, considering the constraints imposed by the spacecraft size. The driving requirement for orbit control is to keep the satellite orbit within a maximum distance of 400 m from the reference orbit. Based on this limitation, a preliminary estimate of the required navigation system accuracy of about 40 m may be considered. Hence, for absolute position determination purposes, it is sufficient to consider a GPS navigation solution in a loosely-coupled GPS/INS integration scheme, capable of providing positioning accuracy of about 20 m. Attitude determination is carried out using star-tracker and three-axis gyro measurements.

The satellite is equipped with the set of actuators summarized in Table 2. A 100 W class Hall effect thruster[15,16] is employed to compensate the secular variation in the orbit semi-major axis, caused by the in-track component of atmospheric drag. Simulation results indicate that the thrust needed to continuously counteract the drag force, for the considered mission scenario, is in the throttling range of such kind of thruster, and comparable to that required in similar missions, like GOCE.[7] A 30 W Xenon resistojet[17] provides out of plane impulsive burns to compensate for the cross-track component of drag, which is due to the co-rotation of the atmosphere with the Earth, and the sun-synchronous resonance effects on the orbit inclination and right ascension of the ascending node. This kind of design is basically a trade-off between the thrust efficiency and the limitations imposed by the satellite payload and available power. In fact, we can take advantage of the Hall thruster high specific impulse to reduce the propellant consumption for drag compensation, which is the dominant factor in the mission delta-v budget, while using a higher thrust, low-power resistojet to counteract smaller cross-track perturbations, at the price of a very low specific impulse. Moreover, a single propellant tank containing Xenon gas will be shared between the Hall effect thruster and the resistojet, resulting in a simplified satellite internal layout. Finally, three momentum wheels produce the torques needed for attitude control. The spacecraft orientation is required to be aligned with the nominal attitude with a maximum absolute error of 0.2° per axis.

C. Spacecraft and power system

In order to assess the feasibility of the proposed propulsion scheme, within the considered mission, a sketch of the spacecraft size, mass and power system is provided.

The external layout of the spacecraft is modeled as a rectangular box, with a square cross-section of 0.5×0.5 m^2 and a length of 1 m or more, similar to the elongated shape of the GOCE spacecraft. The assumed aerodynamic drag coefficient is 2.5.

The total mass of the spacecraft is assumed to be 100 kg, including 12 kg of propellant mass. The Hall thruster, the cathode and the Power Conditioning Unit (PCU) have a mass of less than 3 kg. The mass

Table 2. Actuators

Propulsion	X axis	Y axis	Z axis
Type	100 W HET	30 W R.jet	-
Specific Impulse	∼1000 s	50 s	-
Thrust range	$2.5 - 6$ mN	$10 - 50$ mN	-
Attitude			
Type	1 Momentum Wheel per axis		

of the Xenon resistojet plus its power regulator can be estimated in 1 kg. The tank storing up to 12 liters of Xenon and all the valves, tubing, harness can be limited to additional 3 kg. Therefore, the propulsion system has a dry mass of less than 7 kg. Including the propellant, the whole propulsion system mass will not exceed 20 kg, i.e. about 20% of the total spacecraft mass.

Power is supplied by triple junction solar cells with an efficiency of about 28%, a packing factor of 0.85, and a 3% power degradation over the expected mission life. Given these figures, it is possible to consider solar arrays with a surface area of less than 0.4 m^2 and a mass of about 2 kg, able to provide at least 100 W power at end of life. The external layout of the spacecraft can host a solar array installation of at least 1 m^2, whose total supplied power is largely sufficient for the proposed payload and propulsion needs. A battery system of 150 Wh/kg based on Li-ion cells is feasible for the proposed design.

The Hall thruster system is operated so that the supplied thrust can be changed about every 10 seconds. Several approaches have been proposed in literature in order to provide fast response times for this class of thrusters. Fast flow control valves (e.g. piezoelectric valves or digital MEMS actuators) can be used to quickly change the propellant flow, which in turn provides changes in the thrust (for fixed anode voltage). As an alternative, a high frequency variation (more than 10 Hz), can be obtained by pulse width modulation.[18,19] Thrust variation can also be obtained by operating on the anode voltage through the PCU, at fixed propellant flow rate. This is the approach we refer to in this work and is feasible for the required 0.1 Hz variation rate. Indeed, for the thrust range reported in Table 2, given the Hall thruster technology characteristic, a minimum thrust of 2.5 mN can be obtained with about 40 W power (e.g., 200 V and 0.2 A). A 200 V applied voltage provides a specific impulse of more than 1000 s, as expected. For a 6 mN thrust, one can increase the applied voltage to about 500 V, keeping constant the propellant flow rate, and therefore the current. Then, the specific impulse will significantly increase over the assumed 1000 s.

III. Spacecraft model

This section describes the 6-DoF nonlinear simulation model that has been developed for the proposed mission scenario. This model includes the perturbed translational and rotational spacecraft dynamics, sensors and actuators.

A. Reference frames

Two Earth centered and two spacecraft centered coordinate frames are used in this work for the simulation of point mass and attitude dynamics, respectively. The Earth centered frames are the inertial (ECI) and the Earth fixed (ECEF) frames. The satellite centered frames are the Frenet and body-fixed frames. Vectors with capital letters as superscripts indicate the coordinate frame representation of the vector. Vectors with no superscripts are intended in the inertial reference frame. Rotations between two frames are expressed by rotation matrices $\mathbf{R}$ or quaternions $\mathbf{q}$. The scalar portion of the quaternion is the first element and the quaternion multiplication is defined such that $\mathbf{q}_{AC} = \mathbf{q}_{BC} \circ \mathbf{q}_{AB}$ corresponds to the sequence of rotations $\mathbf{R}_{AC} = \mathbf{R}_{BC}\,\mathbf{R}_{AB}$.

B. Spacecraft dynamics

The simulation model state is a 14-dimensional vector which includes the inertial position $\mathbf{r}$ and velocity $\mathbf{v}$, the quaternion $\mathbf{q}_{IB}$ defining the orientation of the spacecraft with respect to the inertial frame, the spacecraft angular rate $\boldsymbol{\omega}^B$ defined in the spacecraft body reference frame, and the spacecraft mass m. The equations which describe the dynamics of the state vector are:

$$\begin{aligned}
\dot{\mathbf{r}} &= \mathbf{v} \\
\dot{\mathbf{v}} &= -\mu \frac{\mathbf{r}}{\|\mathbf{r}\|^3} + \mathbf{a}_g + \mathbf{a}_d + \mathbf{a}_e + \frac{\mathbf{p}_u}{m} \\
\mathbf{v}^{\uparrow} &= \mathbf{v}^{\downarrow} + \Delta\mathbf{v}_u \\
\dot{\mathbf{q}}_{IB} &= \frac{1}{2}\begin{bmatrix} 0 \\ \boldsymbol{\omega}^B \end{bmatrix} \circ \mathbf{q}_{IB} \\
\dot{\boldsymbol{\omega}}^B &= \mathbf{I}^{-1}\left(\boldsymbol{\tau}_g^B + \boldsymbol{\tau}_d^B + \boldsymbol{\tau}_e^B + \boldsymbol{\tau}_u^B - [\boldsymbol{\omega}^B\times]\,\mathbf{I}\,\boldsymbol{\omega}^B\right) \\
\dot{m} &= -\frac{\|\mathbf{p}_u\|}{g\,I} \\
m^{\uparrow} &= \frac{m^{\downarrow}}{e^{\,\|\Delta\mathbf{v}_u\|/g\,I}}
\end{aligned} \tag{1}$$

The considered orbit disturbance effects are due to the main perturbations acting on spacecrafts at low altitudes.[20] The gravitational and drag perturbations are specified by the disturbance accelerations $\mathbf{a}_g$, $\mathbf{a}_d$ and torques $\boldsymbol{\tau}_g$, $\boldsymbol{\tau}_d$. The minor perturbations are accounted for through the terms $\mathbf{a}_e$ and $\boldsymbol{\tau}_e$. Specifically, a spherical harmonic expansion EGM96[21] up to degree and order 24 for the disturbance acceleration and a spherical mass distribution for the gravity gradient torque are used to model Earth's non-spherical gravity field. The Jacchia-71 model[22] is employed to approximate the atmospheric density, assuming a high solar activity ($F_{10.7} = 220$). The solar radiation pressure takes into account the Earth's orbit eccentricity and eclipse conditions.[23] Magnetic disturbance torques resulting from the interaction of the spacecraft residual magnetic field and the geomagnetic field are described by the IGRF95 model truncated to degree and order 9.[24] Finally, disturbance accelerations due to lunar and solar point mass gravity field are considered, the Sun and Moon position being obtained through precise ephemerides.[13]

C. Sensors

Based on the sensing configuration described in Section B, GPS position measurements are used for absolute position estimation. For attitude determination, combined continuous gyro measurements and discrete star-tracker measurements are employed.[25]

1. GPS

A GPS receiver supplies position measurements to the navigation filter. The measured spacecraft absolute position from the GPS is modeled as the true absolute position (in the ECEF frame) plus white Gaussian noise $\mathbf{w}_r^E$:

$$\check{\mathbf{r}}^E = \mathbf{R}_{IE}\,\mathbf{r} + \mathbf{w}_r^E.$$

The covariance of the GPS noise, in absence of dilution of precision information, is assumed to be $\sigma_r^2\,\mathbf{I}_{3\times3}$.

2. Gyro

The gyro model is based upon a package of three orthogonal strapdown gyros, each measuring the spacecraft angular velocity along its input axis. The input axes are chosen to be coincident with the spacecraft body axes. The measured angular rate $\breve{\boldsymbol{\omega}}^B$ is defined in terms of the true angular rate $\boldsymbol{\omega}^B$ and measurement uncertainties. These include white Gaussian noise $\mathbf{w}_\omega^B$, gyro bias $\mathbf{b}_\omega^B$, scale factor bias f_ω and gyro misalignment $\boldsymbol{\epsilon}_\omega^B$:

$$\breve{\boldsymbol{\omega}}^B = \left(\mathbf{I}_{3\times3} - \left[\boldsymbol{\epsilon}_\omega^B\,\times\right]\right)\left[\,(1+f_\omega)\,\boldsymbol{\omega}^B + \mathbf{b}_\omega^B + \mathbf{w}_\omega^B\,\right].$$

The gyro bias is modeled as a Ornstein-Uhlenbeck process with a large time constant τ_b:[26]

$$\dot{\mathbf{b}}_{\omega}^{B} = -\frac{\mathbf{b}_{\omega}^{B}}{\tau_b} + \mathbf{w}_{bd}^{B}\,. \tag{2}$$

The spectral densities of the white-noise processes $\mathbf{w}_{\omega}^{B}$ and $\mathbf{w}_{bd}^{B}$ are $\sigma_{\omega}^{2}\,\mathbf{I}_{3\times3}$ and $\sigma_{bd}^{2}\,\mathbf{I}_{3\times3}$, respectively.

3. Star-tracker

The star-tracker measures the absolute orientation of the spacecraft. The star-tracker frame is supposed to be aligned with respect to the spacecraft body frame . Sensor noise is modeled as a small rotation vector $\mathbf{w}_{\theta}^{B}$.[26] The output of the star-tracker is thus a quaternion of the form:

$$\breve{\mathbf{q}}_{IB} = \delta\mathbf{q}(\mathbf{w}_{\theta}^{B}) \circ \mathbf{q}_{IB}$$

where $\delta\mathbf{q}(\mathbf{w}_{\theta}^{B}) \approx \left[1\,,\ \mathbf{w}_{\theta}^{B}/2\right]^{T}$ and the measurement noise is suppose to be a white Gaussian process with covariance matrix $\sigma_{\theta}^{2}\,\mathbf{I}_{3\times3}$.

D. Actuators

The satellite is equipped with the set of actuators reported in Table 2: momentum wheels for attitude control and a hybrid electric thruster (Hall effect and resistojet) for translational control. The propulsion system is supposed to be aligned with the satellite body axes, so that control torques and accelerations are uncoupled.

1. Hall effect thruster

A low power Hall effect thruster is employed for the along-track maneuvers. The thrust provided by the Hall effect thruster is obtained from the commanded thrust p_c, considering the following sources of error: actuator noise w_p, scale factor bias f_p and thrust alignment error $\boldsymbol{\epsilon}_{p}^{B}$. The thrust vector, expressed in the inertial reference frame, is:

$$\mathbf{p}_u = \mathbf{R}(\mathbf{q}_{IB}^{*})\left(\mathbf{I}_{3\times3} - \left[\boldsymbol{\epsilon}_{p}^{B}\,\times\right]\right)\begin{bmatrix} (1+f_p)\,p_c + w_p \\ 0 \\ 0 \end{bmatrix}.$$

The thrust noise w_p is modeled as a white Gaussian noise with spectral density σ_{p}^{2}.

2. Resistojet

A low power resistojet, aligned with the cross-track direction, is employed to control the orbital plane inclination and the right ascension of the ascending node. The thrust is applied in short bursts. Other sources of acceleration are considered negligible, so that one burst is approximated by an impulsive velocity change $\Delta\mathbf{v}_u$. The impulsive $\Delta\mathbf{v}_u$ is obtained from the commanded Δv_c, including error sources such as thruster noise $w_{\Delta v}$, scale factor bias $f_{\Delta v}$ and thrust alignment error $\boldsymbol{\epsilon}_{\Delta v}^{B}$:

$$\Delta\mathbf{v}_u = \mathbf{R}(\mathbf{q}_{IB}^{*})\left(\mathbf{I}_{3\times3} - \left[\boldsymbol{\epsilon}_{\Delta v}^{B}\,\times\right]\right)\begin{bmatrix} 0 \\ (1+f_{\Delta v})\,\Delta v_c + w_{\Delta v} \\ 0 \end{bmatrix}.$$

The thrust noise $w_{\Delta v}$ is modeled as a white Gaussian noise with covariance $\sigma_{\Delta v}^{2}$.

3. Momentum wheels

Momentum wheels provide the torques $\boldsymbol{\tau}_{u}^{B}$ needed to change the attitude of the satellite. The considered attitude control strategy requires the generated torques to be independent, with respect to the satellite body axes. Hence there is one momentum wheel per axis. The torque generated by the momentum wheels, for a commanded torque $\boldsymbol{\tau}_{c}^{B}$, includes actuator noise $\mathbf{w}_{\tau}^{B}$, scale factor bias f_τ and misalignment error $\boldsymbol{\epsilon}_{\tau}^{B}$:

$$\boldsymbol{\tau}_{u}^{B} = \left(\mathbf{I}_{3\times3} - \left[\boldsymbol{\epsilon}_{\tau}^{B}\,\times\right]\right)\left[\,(1+f_\tau)\,\boldsymbol{\tau}_{c}^{B} + \mathbf{w}_{\tau}^{B}\,\right].$$

The torque noise $\mathbf{w}_{\tau}^{B}$ is modeled as a white Gaussian noise with spectral density $\sigma_{\tau}^{2}\,\mathbf{I}_{3\times3}$.

IV. Guidance, navigation and control

The proposed GNC system includes autonomous orbit and attitude determination and control algorithms. The navigation solution is based on an extended Kalman filter, which provides estimates of the spacecraft absolute position and attitude. The autonomous orbit control problem is formulated as a leader-follower formation flying control problem in which one spacecraft is virtual and not affected by non-gravitational perturbations.[14] To this aim, a reference trajectory is numerically computed from the nominal orbital elements. An efficient thrusting strategy is then developed using mean orbital elements control theory, while attitude control is carried out using a proportional derivative feedback law. In the following, we provide a brief overview of the proposed GNC system. The interested reader is referred to Ref. 27 for a detailed description.

A. Navigation

A continuous-discrete extended Kalman filter is adopted for autonomous navigation.[28] The filter processes GPS, gyro and star tracker measurements, in order to estimate the position, velocity and attitude of the spacecraft. The state of the filter is a 13-dimensional vector, which includes the inertial position $\hat{\mathbf{r}}$, the inertial velocity $\hat{\mathbf{v}}$, the quaternion $\hat{\mathbf{q}}_{IB}$ defining the orientation of the spacecraft with respect to the inertial frame, and the gyro bias $\hat{\mathbf{b}}_{\omega}^{B}$. Notice that the state vector does not contain angular velocity and mass. In fact, the difference between the gyro output and the estimated gyro bias is used as an estimate of the angular velocity, while the mass is assumed to be directly measured by on-board instruments.

In the prediction step of the filter, a simplified dynamic model of the spacecraft is adopted. Specifically, only the J2 harmonic of the gravity field is explicitly considered, which represent the major perturbing term in (1). Control and drag accelerations are not considered because the resultant from the interaction of the thrust acceleration $\mathbf{p}_u/m$ with the aerodynamic drag $\mathbf{a}_d$ is negligible for the considered mission scenario. The disturbance term $\mathbf{a}_e$ in equation (1), which represents the effects of the minor orbital perturbations, is also neglected.

In the update step of the filter, the attitude estimation error is parametrized by a three-dimensional rotation vector, instead of being expressed in quaternion form. This choice allows one to update the attitude estimates by using a multiplicative approach, while at the same time avoiding covariance singularities due to the quaternion unit-norm constraint.[26]

B. Guidance

Based on the nominal orbit and attitude, the guidance algorithm specifies the desired spacecraft inertial position and velocity, as well as its orientation and angular velocity.

The reference trajectory is computed by integrating the spacecraft dynamic equations. A perturbation term explicitly accounts for the Earth's non-spherical gravity field, modeled using the spherical harmonic expansion EGM96 up to degree and order 9. The initial integration condition is obtained from the initial orbital elements, shown in Table 1. The mean orbital elements are first converted to the corresponding osculating orbit elements, according to Brouwer's artificial satellite theory,[29] then the well-known transformation between osculating orbital elements and inertial states (position, velocity) is applied.[13]

The reference attitude depends only on the current inertial position and velocity of the spacecraft, thus it is independent of the reference trajectory. For attitude control purposes, the reference attitude is expressed as a quaternion corresponding to the orientation of the Frenet reference frame with respect to the inertial reference frame. This quantity can be easily derived from the estimated spacecraft position and velocity.

Analogously, the reference angular rate of the spacecraft has to match the rotation rate of the Frenet frame, expressed in the body frame, which for a nearly circular orbit, is roughly aligned with the Y axis.

C. Control

The orbital station-keeping problem is addressed in a framework based on orbital elements. The control law is formulated in terms of mean orbital elements, rather than osculating orbital elements, so that differential oscillation (with respect to the virtual spacecraft on the reference orbit) due to short periodic gravitational perturbations are not treated as tracking errors.[30] A hybrid continuous/impulsive control scheme is adopted, by taking into account the specific features of the propulsion system and of the considered mission. The in-track continuous thrust provided by the Hall effect thruster is used to control the semi-major axis, the

eccentricity vector, and the mean argument of latitude. To this purpose, a nonlinear feedback regulator is implemented.[31] The inclination and the right ascension of the ascending node are controlled via a cross-track impulsive control scheme provided by the resistojet. To maximize the efficiency of the maneuver, a sequence of impulsive burns at the equatorial or polar region is applied whenever the tracking error exceeds a predefined control window. The sequence is stopped when the error reaches the lower bound of the control window.

Concerning the attitude control, the commanded torques are computed through a classical proportional derivative feedback law. To this purpose, the attitude tracking error is parametrized by the three-dimensional rotation vector obtained from the vector part of the attitude error quaternion.

V. Simulation results

The reference mission has been simulated in order to validate the proposed GNC solution and to evaluate the performance of the hybrid propulsion system. The truth model, navigation state and reference dynamics are propagated using a fourth-order Runge-Kutta integration method. The specifications of sensors and actuators are summarized in Table 3. The standard deviation σ_{bd} of the noise driving the dynamics of the gyro bias (2) has been computed from the standard deviation of the gyro bias σ_b available from the sensor specifications, according to the asymptotic relationship $\sigma_{bd}^2 = 2\sigma_b^2/\tau_b$, with $\sigma_b = 1^\circ/\text{hr}$ and $\tau_b = 2$ hr. The orbit control gains are selected in order to satisfy the Hall thruster output limitations and minimize the

Table 3. Sensors and actuators specifications

Device	Noise	Scale factor	Alignment error	Update frequency
Gyro	$\sigma_\omega = 0.02$ mrad/$\sqrt{\text{s}}$ $\sigma_{bd} = 8.1 \cdot 10^{-8}$ rad/s$^{3/2}$	$f_\omega = 100$ ppm	$\boldsymbol{\epsilon}_\omega^B = 0.3$ mrad/axis	Continuous
Star-tracker	$\sigma_\theta = 0.3$ mrad	-	-	0.05 Hz
Gps	$\sigma_r = 30$ m	-	-	0.1 Hz
Momentum wheels	$\sigma_\tau = 3 \cdot 10^{-5}$ N·m$\sqrt{\text{s}}$	$f_\tau = 300$ ppm	$\boldsymbol{\epsilon}_\tau^B = 0.3$ mrad/axis	Continuous
Hall thruster	$\sigma_p = 0.3$ mN$\sqrt{\text{s}}$	$f_p = 300$ ppm	$\boldsymbol{\epsilon}_\tau^B = 0.3$ mrad/axis	Continuous
Resistojet	$\sigma_{\Delta v} = 1$ mm/s	$f_{\Delta v} = 300$ ppm	$\boldsymbol{\epsilon}_{\Delta v}^B = 0.3$ mrad/axis	Impulsive

steady state oscillations due to estimation errors. The attitude control parameters are found by comparing the linearized attitude dynamics with the second order equation of a mass-spring-damper system and expressing the gains as a function of the natural frequency and damping ratio of the system.[32] The update frequencies of sensors and control algorithms are set to rather conservative values to reduce the power requirement and computational burden of the GNC system.

The performance of the proposed Kalman filtering scheme is evaluated in terms of the inertial position and attitude determination errors. The position determination error is shown together with its 3σ confidence intervals in Figure 1, for the first 60 days of the mission. The filter state is initialized with the first attitude and position measurements. After a short transient phase, each component of the 3σ ECI position vector error drops to a steady state value of approximately 20 m. The error has approximately zero mean and remains within the confidence intervals most of the time.

The closed loop system analysis accounts for the effects of a realistic truth model, sensors, actuators and GNC flight algorithms. Since the orbit control requirements are specified in terms of inertial states, the control system performance is presented, in Figure 2, in terms of osculating position tracking error, even if the control laws are developed in the mean orbital element space. The in-track component of the error, which is proportional to the mean argument of latitude error, has the major impact on the satellite distance from the reference orbit, being controlled passively with an accuracy of about 400 m. The cross-track component is strongly influenced by inclination and right ascension of the ascending node errors: the achieved 250 m accuracy is a function of the impulsive control window size. The normal component is controlled with the accuracy of less than 50 m, reflecting the semi-major axis error. Figure 3 shows the satellite distance from the reference orbit, whose root mean square value is 245 m (neglecting the transient phase). These results show that the control requirements are satisfied.

The performance of the proposed propulsion system is depicted in Figure 4, in terms of the Hall thruster

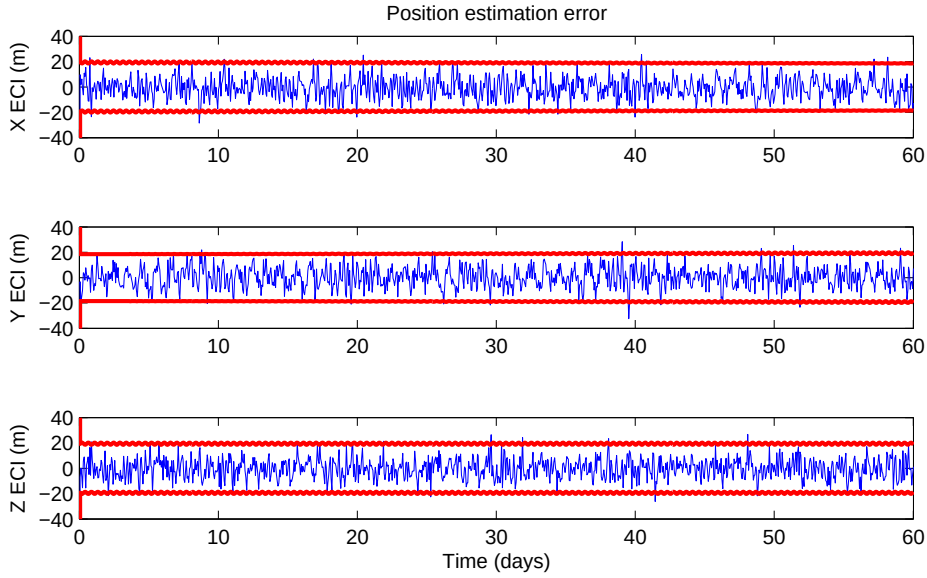

Figure 1. Inertial position estimation error and 3σ confidence intervals.

and resistojet outputs and the Xenon propellant mass consumption. A continuous thrust with mean value of approximately 3.2 mN and delta-v impulses of about 10 mm/s magnitude, which corresponds to a 20 s burn at 50 mN, are required for orbital station-keeping. In the second plot of Figure 4, each burn is represented by a bullet. An increased density of bullets in the plot indicates that the resistojet is firing twice per orbit rather than once, while the thruster is not firing in correspondence of empty spaces. Note that the power requirements for simultaneous use of the resistojet and the Hall thruster is about 140 W, which is fully compatible with the power system described in Section C. The total propellant consumption is 3.08 kg, including 1.65 kg for continuous thrust and 1.43 kg for impulsive maneuvers. Considering a 12 kg propellant tank, simulations show that the expected lifetime of the satellite is approximately 226 days.

VI. Conclusions

The paper has analyzed the performance of a hybrid electric propulsion system for autonomous station keeping in a LEO mission. The results demonstrate the viability of the proposed solution, in terms of both accuracy of the GNC scheme and performance of the propulsion system.

Future work will concern performance analysis of the hybrid propulsion scheme within different types of missions, including formation flying control. The use of parametric models for the thrust profile and of optimal control techniques for the minimization of the power consumption will be also the subject of future investigations.

References

[1]Oleson, S. R., Myers, R. M., Kluever, C. A., Riehl, J. P., and Curran, F. M., "Advanced Propulsion for Geostationary Orbit Insertion and North-South Station Keeping," *Journal of Spacecraft and Rockets*, Vol. 34, No. 1, 1997, pp. 22–28, doi: 10.2514/2.3187.

[2]Romero, P., Gambi, J. M., Patio, E., and Antolin, R., "Optimal Station Keeping for Geostationary Satellites with Electric Propulsion Systems Under Eclipse Constraints," *Progress in Industrial Mathematics at ECMI 2006*, Vol. 12 of *Mathematics in Industry*, Springer-Verlag, Berlin, Germany, 2008, pp. 260–264, doi: 10.1007/978-3-540-71992-2_31.

[3]Mailhe, L. M. and Heister, S. D., "Design of a Hybrid Chemical/Electric Propulsion Orbital Transfer Vehicle," *Journal of Spacecraft and Rockets*, Vol. 39, No. 1, 2002, pp. 131–139, doi: 10.2514/2.3791.

[4]Manzella, D., "Low Cost Electric Propulsion Thruster for Deep Space Robotic Missions," *2007 NASA Science Technology Conference*, Hyattsville, Maryland, June 2007, Paper No. 07-0116.

[5]Patel, P., Scheeres, D., and Gallimore, A., "Maximizing Payload Mass Fractions of Spacecraft for Interplanetary Electric

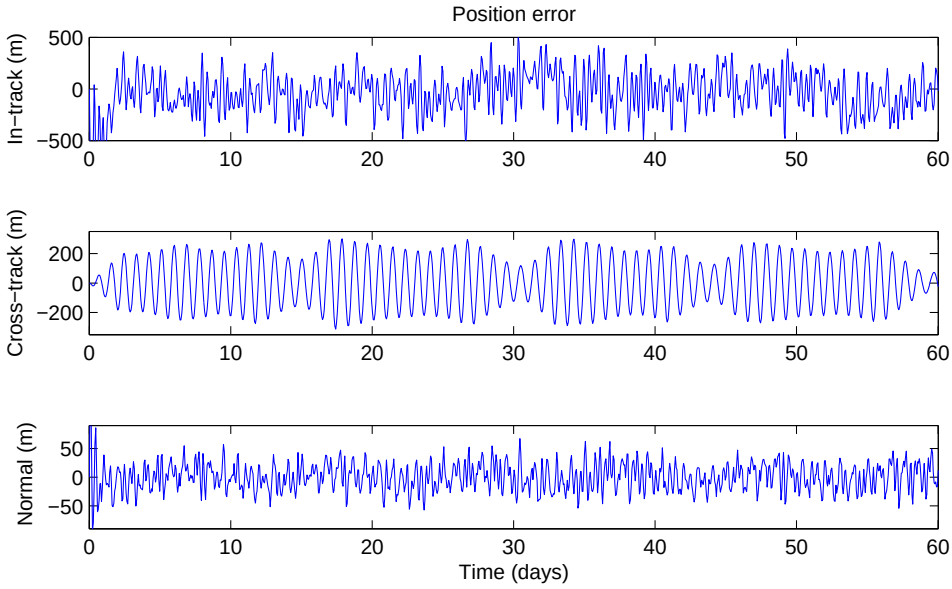

Figure 2. Position tracking error.

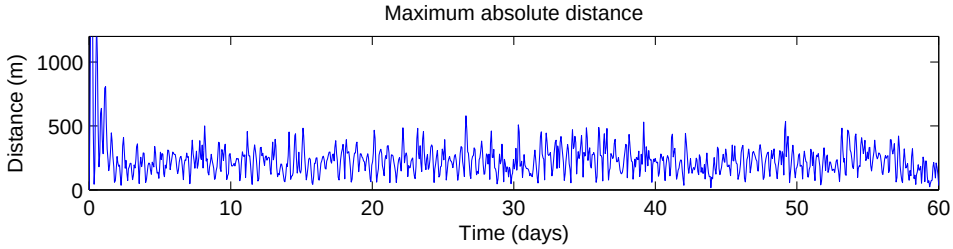

Figure 3. Distance from the reference orbit.

Propulsion Missions," *Journal of Spacecraft and Rockets*, Vol. 43, No. 4, 2006, pp. 822–827, doi: 10.2514/1.17433.

[6]Muzi, D. and Allasio, A., "GOCE: The First Core Earth Explorer of ESA's Earth Observation Programme," *Acta Astronautica*, Vol. 54, No. 3, 2004, pp. 167–175, doi: 10.1016/S0094-5765(02)00296-5.

[7]Canuto, E. and Massotti, L., "All-propulsion design of the drag-free and attitude control of the European satellite GOCE," *Acta Astronautica*, Vol. 64, No. 2-3, 2009, pp. 325 – 344, doi: 10.1016/j.actaastro.2008.07.017.

[8]Fleck, M. E. and Starin, S. R., "Evaluation of a Drag-free Control Concept for Missions in Low Earth Orbit," *AIAA Guidance, Navigation, and Control Conference and Exhibit*, Paper No. 03-5747, Austin, Texas, August 2003.

[9]Blandino, J., Marchetti, P., and Demetriou, M., "Electric Propulsion and Controller Design for Drag-Free Spacecraft Operation," *Journal of Spacecraft and Rockets*, Vol. 45, No. 6, 2008, pp. 1303–1315, doi: 10.2514/1.36307.

[10]Fearn, D., "Economical Remote Sensing from a Low Altitude with Continuous Drag Compensation," *Acta Astronautica*, Vol. 56, No. 5, 2005, pp. 555–572, doi: 10.1016/j.actaastro.2004.09.052.

[11]Königsmann, H. J., Collins, J. T., Dawson, S., and Wertz, J. R., "Autonomous Orbit Maintenance System," *Acta Astronautica*, Vol. 39, No. 9-12, 1996, pp. 977–985, doi: 10.1016/S0094-5765(97)00084-2.

[12]Boain, R. J., "A-B-Cs of Sun-Synchronous Orbit Mission Design," *Spaceflight Mechanics 2004*, Vol. 119 of *Advances in the Astronautical Sciences Series*, Univelt, Incorporated, San Diego, California, 2005, pp. 85–104.

[13]Vallado, D. A., *Fundamental of Astrodynamics and Applications*, Microcosm Press, El Segundo, California, 2nd ed., 2001.

[14]De Florio, S. and D'Amico, S., "Optimal Autonomous Orbit Control of a Remote Sensing Spacecraft," *Spaceflight Mechanics 2009*, Vol. 134 of *Advances in the Astronautical Sciences Series*, Univelt, Incorporated, San Diego, California, 2009, pp. 949–968.

[15]Polzin, K. A., Markusic, T. E., Stanojev, B. J., DeHoyos, A., Raitses, Y., Smirnov, A., and Fisch, N. J., "Performance of a Low-Power Cylindrical Hall Thruster," *Journal of Propulsion and Power*, Vol. 23, No. 4, 2007, pp. 886–888, doi: 10.2514/1.28595.

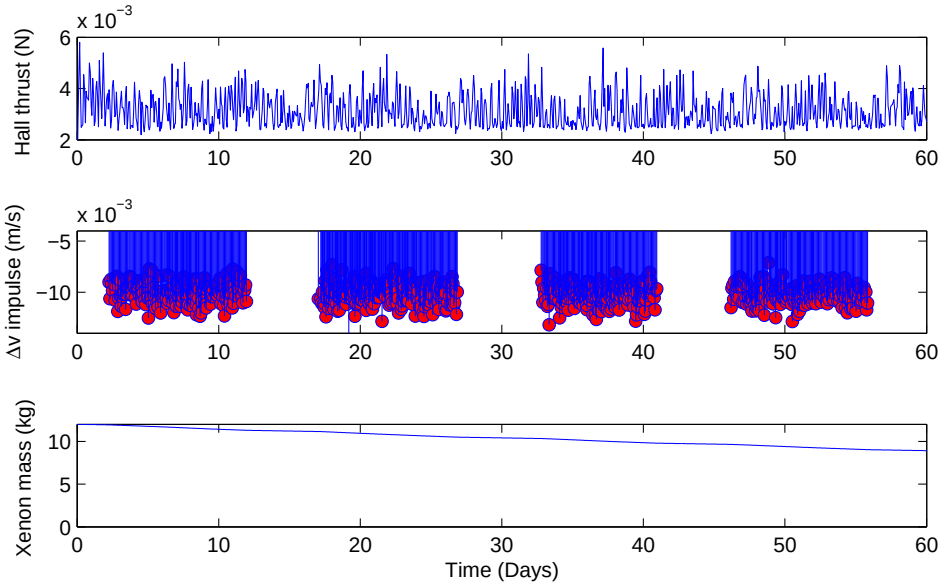

Figure 4. Propulsion system performance.

[16]Loyan, A. V. and Maksymenko, T. A., "Performance Investigation of SPT-20M Low Power Hall Effect Thruster," *Journal of Technical Physics*, Vol. 49, No. 3-4, 2008, pp. 283–302.

[17]Nicolini, D., Robertson, D., Chesta, E., Saccoccia, G., Gibbon, D., and Baker, A. M., "Xenon resistojets as a secondary propulsion on EP spacecrafts and performance results of resistojets using Xenon," *28th International Electric Propulsion Conference*, Toulouse, France, March 2003, Paper No. 03-305.

[18]Hruby, V., Pote, B., Gamero-Castao, M., Kolencik, G., Byrne, L., Tedrake, R., and Delichatsios, M., "Hall Thrusters Operating in Pulsed Mode," *27th International Electric Propulsion Conference*, Pasadena, California, October 2001, Paper No. 01-66.

[19]Rossetti, P. and Valentian, D., "Analysis of Hall-Effect Thrusters Application to Formation Flying and Drag Compensation," *30th International Electric Propulsion Conference*, Florence, Italy, September 2007, Paper No. 07-307.

[20]King-Hele, D., *Satellite orbits in an atmosphere: theory and applications*, Blackie and Son Ltd, London, United Kingdom, 1987.

[21]Lemoine, F. G., Kenyon, S. C., Factor, J. K., Trimmer, R., Pavlis, N. K., Chinn, D. S., Cox, C. M., Klosko, S. M., Luthcke, S. B., Torrence, M. H., Wang, Y. M., Williamson, R. G., Pavlis, E. C., Rapp, R. H., and Olson, T. R., "The Development of the Joint NASA GSFC and the NIMA Geopotential Model EGM96," Tech. rep., NASA/TP-1998-206861, 1998.

[22]Jacchia, L. G., "Revised Static Models of the Thermosphere and Exosphere with Empirical Temperature Profiles," Tech. Rep. 332, Smithsonian Astrophysical Observatory, 1971.

[23]Montenbruck, O. and Gill, E., *Satellite Orbits*, Springer-Verlag, Berlin, Germany, 2000.

[24]Barton, C., "International Geomagnetic Reference Field: The Seventh Generation," *Journal of Geomagnetism and Geoelectricity*, Vol. 49, No. 2-3, 1997, pp. 123–148.

[25]Woffinden, D. C. and Geller, D. K., "Relative Angles-Only Navigation and Pose Estimation for Autonomous Orbital Rendezvous," *Journal of Guidance, Control, and Dynamics*, Vol. 30, No. 5, 2007, pp. 1455–1469, doi: 10.2514/1.28216.

[26]Pittelkau, M. E., "Rotation Vector in Attitude Estimation," *Journal of Guidance, Control, and Dynamics*, Vol. 26, No. 6, 2003, pp. 855–860, doi: 10.2514/2.6929.

[27]Garulli, A., Giannitrapani, A., Leomanni, M., and Scortecci, F., "Autonomous Low Earth Orbit Station-Keeping with Electric Propulsion," Tech. Rep. 2011-1, Dipartimento di Ingegneria dell'Informazione, Università di Siena, 2011.

[28]Crassidis, J. L. and Junkins, J. L., *Optimal Estimation of Dynamic Systems*, Chapman & Hall/CRC press, Boca Raton, Florida, 2004.

[29]Brouwer, D., "Solution of the Problem of Artificial Satellite Theory Without Drag," *The Astronomical Journal*, Vol. 64, No. 1274, 1959, pp. 378–396, doi: 10.1086/107958.

[30]Schaub, H., Vadali, S. R., Junkins, J. L., and Alfriend, K. T., "Spacecraft Formation Flying Control Using Mean Orbit Elements," *Journal of the Astronautical Sciences*, Vol. 48, No. 1, 2000, pp. 69–87.

[31]Gurfil, P., "Control-Theoretic Analysis of Low-Thrust Orbital Transfer Using Orbital Elements," *Journal of Guidance, Control, and Dynamics*, Vol. 26, No. 6, 2003, pp. 979–983, doi: 10.2514/2.6926.

[32]Wertz, J. R., *Spacecraft attitude determination and control*, Reidel Publishing Company, Dordrecht, Holland, 1978.